Electronic structure of YFe_2Ge_2 studied by angle-resolved photoemission spectroscopy

D. F. Xu,[1,2,3] D. W. Shen,[4,5,*] D. Zhu,[6] J. Jiang,[1,2,3] B. P. Xie,[1,2,3] Q. S. Wang,[1] B. Y. Pan,[1] P. Dudin,[7] T. K. Kim,[7] M. Hoesch,[7] J. Zhao,[1,3] X. G. Wan,[6] and D. L. Feng[1,2,3,†]

[1]*State Key Laboratory of Surface Physics, Department of Physics, Fudan University, Shanghai 200433, China*
[2]*Laboratory of Advanced Materials, Fudan University, Shanghai 200433, China*
[3]*Collaborative Innovation Center of Advanced Microstructures, Fudan University, Shanghai 200433, China*
[4]*State Key Laboratory of Functional Materials for Informatics, Shanghai Institute of Microsystem and Information Technology (SIMIT), Chinese Academy of Sciences, Shanghai 200050, China*
[5]*CAS-Shanghai Science Research Center, Shanghai 201203, China*
[6]*National Laboratory of Solid State Microstructures, Collaborative Innovation Center of Advanced Microstructures, and College of Physics, Nanjing University, Nanjing 210093, China*
[7]*Diamond Light Source, Harwell Science and Innovation Campus, Didcot OX11 0DE, United Kingdom*

(Received 29 August 2015; revised manuscript received 17 December 2015; published 11 January 2016)

We report an angle-resolved photoemission spectroscopy study of a $ThCr_2Si_2$-type superconductor YFe_2Ge_2 ($T_c \approx 1.8$ K) in the normal state. The resolved low-energy band structure mainly consists of several flat Fe bands, while the renormalization factors of different bands range from 1.7 to 2.8. Around the Fermi level, these bands contribute to a high density of states, which may account for the unusually high Sommerfeld coefficient γ. Besides, a 30 meV kink is observed, which is probably induced by electron-phonon interactions. Our results indicate that YFe_2Ge_2 is a moderately correlated compound, while electron-phonon coupling should be taken into account to better understand its properties.

DOI: 10.1103/PhysRevB.93.024506

I. INTRODUCTION

The recent discovery of superconductivity in YFe_2Ge_2 ($T_c \approx 1.8$ K) has stimulated many research interests [1–6]. Similar to the 122 family of iron-based superconductors, YFe_2Ge_2 crystallizes in a $ThCr_2Si_2$ structure ($I4/mmm$) [Fig. 1(a)], in which FeGe layers are stacked along the c axis with alternating layers of yttrium ions. On the other hand, the isostructural compound $LuFe_2Ge_2$ exhibits antiferromagnetic spin density wave order below 9 K. Through partially substituting lutetium by yttrium, the transition is continuously suppressed, with the magnetic quantum critical point (QCP) lying near a critical composition of $Lu_{0.8}Y_{0.2}Fe_2Ge_2$ [7]. For YFe_2Ge_2, evidence of fluctuating spin moments on the iron sites has been found in the core level photoemission spectroscopy experiment [2]. First-principles calculations further predicted that there exist competing magnetic interactions in this compound [5]. In this context, several possible superconducting pairing mechanisms have been proposed, including sign-changing $s_\pm$ wave singlet pairing [5] and spin fluctuation mediated triplet pairing [6]. Moreover, the Sommerfeld coefficient of YFe_2Ge_2 reaches an unusually high value ($\sim$100 mJ/mol K^2) for a d-electron compound [1,3], which makes YFe_2Ge_2 even more intriguing.

To reach a better understanding of YFe_2Ge_2, a comprehensive study of its electronic structure is a prerequisite. In this paper, we report an angle-resolved photoemission spectroscopy (ARPES) study of YFe_2Ge_2 in the normal state. The observed low-energy band structure is mainly contributed by five Fe bands, three of which intersect the Fermi level (E_F), forming two hole pockets around the zone center and one electron pocket around the zone corner. The renormalization factors of different bands are around 1.7–2.8, indicating that electronic correlations are moderate in this compound. Around E_F, these bands contribute to a high density of states, which may account for the unusually high Sommerfeld coefficient γ. Furthermore, we find a kink around 30 meV in the band dispersion, which may be attributed to strong electron-phonon interactions. Our results put constraints on theory and lay the foundation for further investigations of this compound.

II. SAMPLE PROPERTIES AND EXPERIMENTAL SETUP

High quality YFe_2Ge_2 single crystals were synthesized from tin flux, as described elsewhere [8]. For as-grown crystals, the electron probe microanalysis gives an average composition of Y:Fe:Ge = 1.000:2.115:1.920. Figure 1(b) presents the x-ray diffraction (XRD) pattern. The narrow peak width in the rocking scan curve guarantees the high crystalline quality of the single crystal [inset of Fig. 1(b)]. YFe_2Ge_2 is metallic over a wide temperature range (2.5–300 K) and the resistivity data show that the residual resistivity ratio RRR = ρ(300 K)/ρ(2.5 K) is typically about 37 [Fig. 1(c)]. The superconductivity in YFe_2Ge_2 is rather sensitive to the sample quality [3,4]. For our samples, a sharp superconducting transition (around 1.8 K) is only observed in powder [inset of Fig. 1(c)]. In Fig. 1(d), the specific heat data are plotted in the form of C_p/T vs T^2. By fitting the low temperature data (6–11 K) with the formula $C_p/T = \gamma + \beta_3 T^2 + \beta_5 T^4$, the Sommerfeld coefficient γ is extrapolated to be 96 mJ/mol K^2, while β_3 is approximately 2.95×10^{-2} mJ/mol K^4. From the value of β_3, we estimate the Debye temperature as $\Theta_D \approx 403$ K. All these transport properties are qualitatively consistent with previous reports [1–4,8].

ARPES measurements were performed at Beamline I05-ARPES of the Diamond Light Source in which a VG-Scienta

*dwshen@mail.sim.ac.cn
†dlfeng@fudan.edu.cn

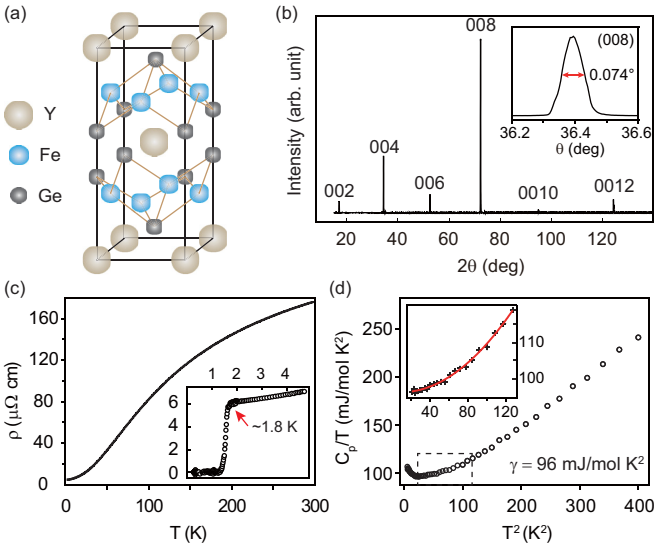

FIG. 1. The crystallographic and transport properties of YFe_2Ge_2. (a) Representative unit cell of YFe_2Ge_2. (b) The x-ray diffraction pattern of the single crystal. The full width at half maximum (FWHM) of the (008) peak in the rocking scan is about 0.074°. (c) The temperature dependence of the electrical resistivity of the single crystal (from 2.5 to 300 K). Resistivity data for powder at even lower temperatures are shown in the inset, showing a superconducting transition at 1.8 K. (d) The specific heat data of YFe_2Ge_2 divided by temperature vs temperature squared. The Sommerfeld coefficient is obtained by fitting the data at low temperatures, which are shown in the inset.

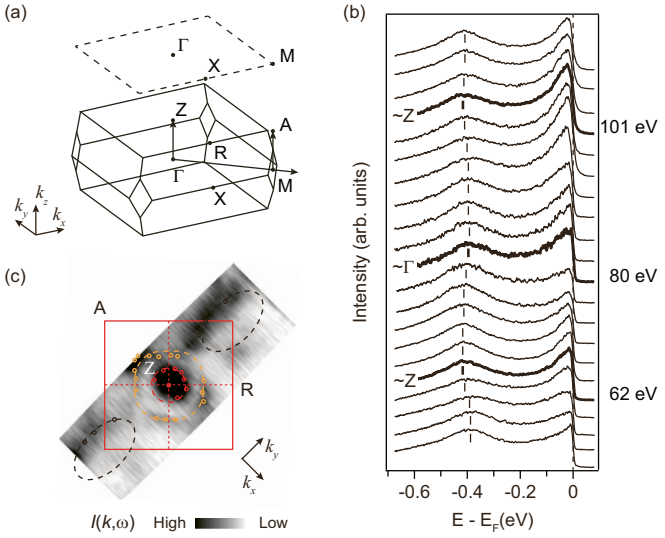

FIG. 2. (a) The three-dimensional BZ of YFe_2Ge_2. The dashed lines represent the two-dimensional plot of the simplified BZ. (b) Photon-energy-dependent EDCs recorded at normal emission. (c) The photoemission intensity map integrated over $[E_F - 5$ meV, $E_F + 5$ meV], which is taken with circularly polarized 104 eV photons (around the Z point). The open circles are Fermi crossings determined by the corresponding MDCs. The dashed lines are guides to the eye for the Fermi surface contours. Data were taken at 7 K.

R4000 electron analyzer is equipped. The typical angular resolution is 0.2° and the overall energy resolution is better than 20 meV for the photon energies used. Samples were cleaved *in situ* and measured under an ultrahigh vacuum of better than 8×10^{-11} Torr.

III. EXPERIMENTAL RESULTS

The three-dimensional Brillouin zone (BZ) of YFe_2Ge_2 is illustrated in Fig. 2(a). To determine the correspondence between the typical photon energies and the high-symmetry points, we plot the energy distribution curves (EDCs) recorded at normal emission as a function of photon energy [Fig. 2(b)]. A wide range of photon energies is used here to cover more than one whole BZ along the k_z direction. A periodic variation of the peak positions for the band around −400 meV can be observed. Using the free electron final-state model [9] with an inner potential of 12 eV, we estimate 80 eV for the ΓXM plane, and 62/101 eV for the ZRA plane.

Next, we examine the low-lying band structure of YFe_2Ge_2 along high-symmetry directions. The photoemission intensity plots taken around the ZRA plane are presented in Figs. 3(a) and 3(d). Along Z-A, by tracking the peaks in the corresponding EDCs around the zone center [Fig. 3(b)], two bands assigned as α and γ can be resolved around −20 and −400 meV, respectively. From the momentum distribution curves (MDCs) near E_F, one holelike band can be distinguished to cross E_F [Fig. 3(c)]. It further disperses backwards to E_F around the zone corner [Fig. 3(b)], and we

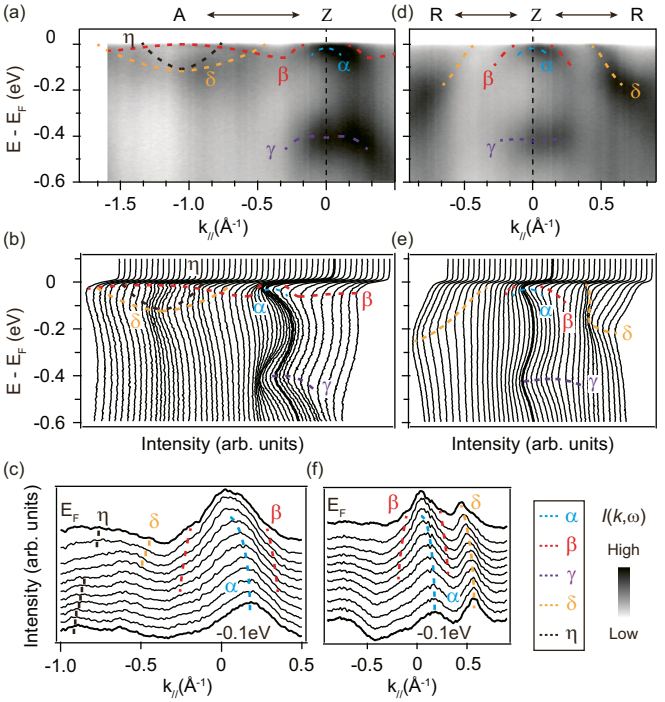

FIG. 3. The photoemission data taken around the Z point. (a) The photoemission intensity plot taken with 101 eV circularly polarized photons along the Z-A direction. (b) The corresponding EDCs for the data in (a). (c) The corresponding MDCs for the data in (a). (d)–(f) The same as those in (a)–(c), but taken along the Z-R direction. Dashed lines are guides for the eye for band dispersions. Data were taken at 7 K.

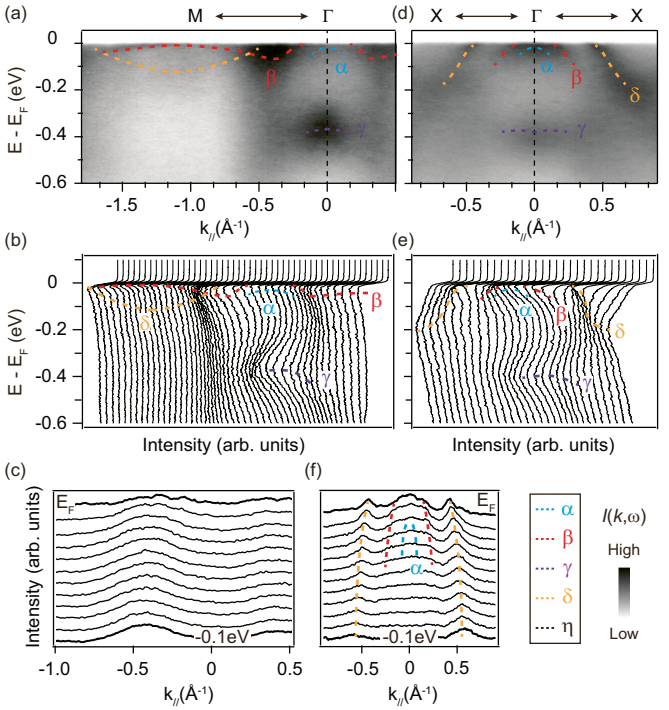

FIG. 4. The photoemission data taken around the Γ point. (a) The photoemission intensity plot taken with 80 eV circularly polarized photons along the Γ-M direction. (b) The corresponding EDCs for the data in (a). (c) The corresponding MDCs for the data in (a). (d)–(f) The same as those in (a)–(c), but taken along the Γ-X direction. Dashed lines are guides for the eye for band dispersions. Data were taken at 7 K.

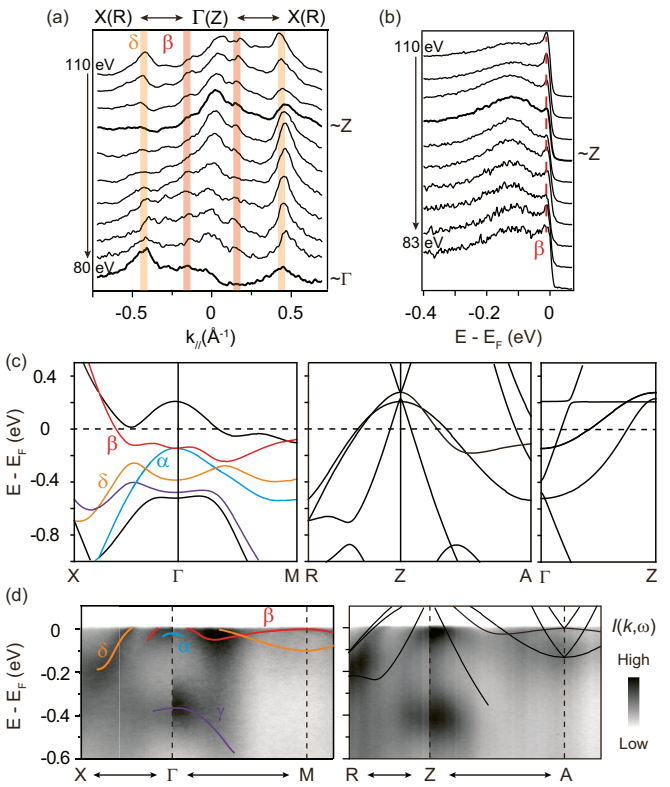

FIG. 5. The three-dimensional band structure of YFe_2Ge_2. (a) The photon-energy dependence of the MDCs integrated over $[E_F - 5$ meV, $E_F + 5$ meV$]$ along Γ(Z)-X(R). (b) The photon-energy dependence of the EDCs at M(A). (c) The band calculations along high-symmetry directions, showing the highly three-dimensional nature of the band structure. (d) The corresponding band structure along high-symmetry directions. Along $X\Gamma M$, solid lines are guides to the eye for the band dispersions. Along RZA, the calculated band dispersions are renormalized by a factor of 2.5 and overlaid on the photoemission intensity plot for comparison.

assign this band as β. Around the A point, we can find one more holelike band with a larger Fermi crossing and an electronlike band from the corresponding EDCs and MDCs [Figs. 3(b) and 3(c)]. These two bands are assigned as δ and η, respectively. Along Z-R, β and δ cross E_F, forming two hole pockets, while α sinks below E_F [Figs. 3(d)–3(f)]. Thus, as depicted in Fig. 2(c), the resulting Fermi surface consists of one circular hole pocket, one rounded rectangle hole pocket around the zone center, and one elliptical electron pocket around the zone corner. The strong intensity at the zone center corresponds to the residual spectral weight of α, which leads to some additional peaks around E_F in the corresponding MDCs as well [Figs. 3(c) and 3(f)].

In Fig. 4, we present the photoemission data taken around the ΓXM plane. The detailed EDCs and MDCs are shown in Figs. 4(b), 4(c), 4(e), and 4(f), respectively. Except for an intensity variation of some bands, the band structure observed here roughly coincides with that around the ZRA plane. Especially, the band dispersions along Γ-X are almost identical to those along Z-R [Figs. 3(d) and 4(d)]. In Figs. 5(a) and 5(b), we present the photon-energy dependence of the MDCs integrated along Γ(Z)-X(R) and the EDCs at the M(A) point. Only a weak variation of the peak positions upon varying the photon energies is observed, indicating that the electronic structure is quasi-two-dimensional. Here, we emphasize that our measured data do not originate from surface states since surface states should be purely two dimensional and no periodicity of the band(s) upon changing photon energy could be found. However, according to the calculations [5,6], the electronic structure of YFe_2Ge_2 is highly three dimensional. In Fig. 5(c), we present the band calculations along $X\Gamma M$ and RZA for comparison. It turns out that the measured band structure around the ΓXM plane qualitatively agrees with the calculations after shifting and renormalizing bands along the energy axis, while that around the ZRA plane does not. To be specific, there are no linear dispersing bands observed in the experiment which are predicted by the calculations, while there are no calculated bands corresponding to the intensity around −400 meV along RZA. Assuming that the calculations are accurate, the discrepancies might be attributed to the following reasons. The first one is the matrix element effect, which may lead to the absence of some typical bands if the matrix element vanishes due to the polarization or energy of the photons or even the experimental geometry. The second one is the limited k_z resolution of ARPES with vacuum ultraviolet photons. This means that bands from a specific k_z plane may have a projection over a wide range of k_z's. For the photon energies we used here, we estimate that the photoelectron escape depth λ is about 5 Å [10]. This corresponds to an intrinsic broadening

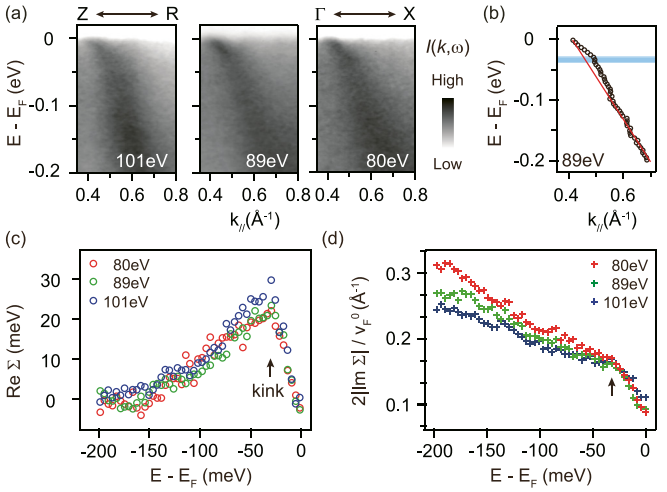

FIG. 6. The analysis of the kink. (a) The magnified photoemission intensity plot around the kink taken with circularly polarized 101, 89, and 80 eV photons, respectively. (b) The dispersion of the δ band (89 eV) obtained by fitting the corresponding MDCs. The red dashed line is obtained by fitting the high-energy dispersion linearly. The blue thick line roughly indicates the mode energy. (c), (d) The self-energy analysis of the kink structure.

of the electron momentum component perpendicular to the sample surface $\delta k_\perp = 1/\lambda \sim 0.2$ Å^{-1}, which is about 16% of the length of the BZ ($4\pi/c \sim 4 \times 3.14/10.42$–$1.2$ Å^{-1}). We note that such broadening may not be sufficient to account for the situation observed here. Other broadening effects or the validity of the band calculations are yet to be explored.

It is worth noting that a kinklike feature is observed in the dispersion of the δ band along $\Gamma(Z)$-$X(R)$ [Fig. 6(a)], which is a typical manifestation of strong electron-boson coupling. This kink is observed across the whole BZ along k_z. We select the data in three typical k_z planes, the ZRA plane (101 eV), the ΓXM plane (80 eV), and an intermediate k_z plane (89 eV) as representatives for the analyses below. We extract the dispersion of δ from the corresponding MDCs [as exemplified in Fig. 6(b)]. The high-energy dispersion is fitted linearly and used as an approximation of the bare band dispersion without an electron-boson interaction [11,12]. The kink is located at around 30 meV [Fig. 6(b)], which coincides with the Debye temperature extrapolated from our transport data, $\Theta_D \approx 403$ K ($k_B\Theta_D \approx 34.7$ meV). This coincidence suggests that the kink might be induced by electron-phonon coupling. Following the common practice in ARPES [11–13], we subtract the bare band dispersion from the experimental one to evaluate the real part of the self-energy $\Sigma(\omega)$ [Fig. 6(c)]. The imaginary part of $\Sigma(\omega)$ over the Fermi velocity of the bare band is approximated by the full width at half maximum of the Lorenztian peaks used to fit the MDCs [Fig. 6(d)]. Around 30 meV, there are clear peaks in the Re $\Sigma(\omega)$ and rapid decreases in the $|2\,\mathrm{Im}\,\Sigma(\omega)|$ for all the representative k_z's, as expected in the presence of electron-phonon coupling. Based on the gradient of the experimental Re $\Sigma(\omega)$ near E_F, the coupling parameter can be estimated to be $\lambda = 1.19 \pm 0.14$ (101 eV), 1.03 ± 0.10 (89 eV), and 0.94 ± 0.11 (80 eV), respectively. The enhancement of the FWHM of the Lorenztian peaks is due to the electron correlations resembling those observed in pnictides [13,14]. The large background may be attributed to the inelastic scattering induced by impurity or the nearness to a magnetic QCP.

Here, we note that the kink is only clearly observed in the δ band. However, we cannot exclude the possibility of kinklike features in other bands' dispersion. For YFe_2Ge_2, except for the δ band, other bands in the vicinity of E_F are all rather flat, which may hinder the observation of a kink. Furthermore, the proximity of these bands makes it challenging to determine precisely the band dispersions.

IV. DISCUSSION AND CONCLUSION

To obtain the information of the electronic correlation strength of YFe_2Ge_2, we renormalize the bands given by calculations to fit those observed by ARPES and summarize the results in Fig. 5(d). Quantitatively, around the ΓXM plane, the renormalization factors for different bands are around 1.7–2.1, while around the ZRA plane, the overall renormalization factors are about 2.4–2.8. For comparison, the renormalization factor of $BaFe_2As_2$ is around 2–3 [15–17]. From an ionic picture, the Fe electron occupation (given by calculations) in YFe_2Ge_2 is $3d^{6.5}$ [5]. The larger occupation number of electrons than that in $BaFe_2As_2$ ($3d^6$) weakens the Hund's interaction, leading to reduced electron correlations. Moreover, the Fe-Ge bond length (2.393 Å) is found to be smaller than the Fe-As bond length (2.403 Å), which favors electron hopping. The above qualitative analysis suggests that the overall correlation strength of YFe_2Ge_2 should be weaker than that of $BaFe_2As_2$. Consistently, for materials with a higher electron occupation, for instance, $BaNi_2As_2$ ($3d^8$) and KNi_2Se_2 ($3d^{8.5}$), the renormalization factors monotonically decrease to 1.66 and 1.54, respectively [18,19].

This moderate electron correlation of YFe_2Ge_2 seems to be in contradiction to its high Sommerfeld coefficient. Such behavior has also been reported in $TlNi_2Se_2$ and KNi_2Se_2 [19,20], which has been explained by a rather large density of states at E_F. Following the same procedure described in Ref. [19], we use our photoemission data to estimate the γ coefficient by the formula $\gamma \propto \sum_n \int_{s_n(E_F)} \frac{ds}{|\nabla_k E(k_F)|}$, in which n is the band index, ds is the perimeter of the Fermi surface, and $|\nabla_k E(k_F)|$ is the Fermi velocity at E_F. We use the 104 eV data in which the band structure is better defined and simplify the estimation by regarding the system as a quasi-two-dimensional one. The obtained $\sum_n \int_{s_n(E_F)} \frac{ds}{|\nabla_k E(k_F)|}$ is about 22.2 eV^{-1} Å^{-2}. Through interpolation [19], the γ is extracted to be roughly 67 mJ/mol K^2, which is in rough agreement with the one obtained in the specific heat measurement (96 mJ/mol K^2). This indicates that the large Sommerfeld coefficient should be attributed to the high density of states at E_F as well. The underestimation of γ by our photoemission data might be caused by the following reasons. First, due to the overwhelming intensity of α, we may miss the extra Fermi surface contributed by δ around the zone center [Fig. 5(d)], which may also contribute a sizable density of states at E_F. Second, although α sinks below E_F, its broad linewidth of EDCs suggests that there exists a certain amount

of states at E_F, which we have not taken into account in our simplified estimation.

Recent neutron scattering experiments detected two coexisting magnetic fluctuations in YFe_2Ge_2 at low temperatures [21], namely, A-type and stripe antiferromagnetic fluctuations, providing evidence that the superconductivity may be mediated by spin fluctuations. However, with a sizable density of states at E_F, the speculation that the superconductivity is mediated by an electron-phonon interaction also makes sense. In this regard, YFe_2Ge_2 resembles $2H$-$NbSe_2$ (a conventional superconductor with $T_c = 7.2$ K) in the sense that they share a similar electron-phonon coupling strength and mode energy [22]. Further investigations are required to distinguish these different scenarios.

To summarize, we report an ARPES study of YFe_2Ge_2 in the normal state. The electronic correlations are moderate in this compound. Moreover, we find a 30 meV boson mode in the band structure, which is most probably caused by electron-phonon coupling. Our results put constraints on theory and lay the foundation for further investigations of this compound.

ACKNOWLEDGMENTS

We thank the Diamond Light Source for access to Beamline I05-ARPES (Proposal No. SI10213) that contributed to the results presented here. This work is supported in part by the National Science Foundation of China and National Basic Research Program of China (973 Program) under Grants No. 2012CB921402, No. 2012CB927401, No. 11274332, and No. 11227902. D.W.S. is also supported by the "Strategic Priority Research Program (B)" of the Chinese Academy of Sciences (Grant No. XDB04040300).

[1] Y. Zou, Z. Feng, P. W. Logg, J. Chen, G. I. Lampronti, and F. M. Grosche, Phys. Status Solidi **8**, 928 (2014).
[2] N. Sirica, F. Bondino, S. Nappini, I. Píš, L. Poudel, A. D. Christianson, D. Mandrus, D. J. Singh, and N. Mannella, Phys. Rev. B **91**, 121102(R) (2015).
[3] H. Kim, S. Ran, E. D. Mun, H. Hodovanets, M. A. Tanatar, R. Prozorov, S. L. Bud'ko, and P. C. Canfield, Philos. Mag. **95**, 804 (2015).
[4] J. S. Chen, K. Semeniuk, Z. Feng, P. Reiss, Y. Zou, P. W. Logg, G. I. Lampronti, and F. M. Grosche, arXiv:1507.01436.
[5] A. Subedi, Phys. Rev. B **89**, 024504 (2014).
[6] D. J. Singh, Phys. Rev. B **89**, 024505 (2014).
[7] S. Ran, S. L. Bud'ko, and P. C. Canfield, Philos. Mag. **91**, 4388 (2011).
[8] M. Avila, S. Bud'ko, and P. Canfield, J. Magn. Magn. Mater. **270**, 51 (2004).
[9] S. Hüfner, in *Photoelectron Spectroscopy*, 3rd ed. (Springer, New York, 2003), pp. 39–60.
[10] J. Krempasky, V. N. Strocov, L. Patthey, P. R. Willmott, R. Herger, M. Falub, P. Blaha, M. Hoesch, V. Petrov, M. C. Richter, O. Heckmann, and K. Hricovini, Phys. Rev. B **77**, 165120 (2008).
[11] P. Richard, T. Sato, K. Nakayama, S. Souma, T. Takahashi, Y.-M. Xu, G. F. Chen, J. L. Luo, N. L. Wang, and H. Ding, Phys. Rev. Lett. **102**, 047003 (2009).
[12] X. Y. Cui, K. Shimada, Y. Sakisaka, H. Kato, M. Hoesch, T. Oguchi, Y. Aiura, H. Namatame, and M. Taniguchi, Phys. Rev. B **82**, 195132 (2010).
[13] L. Wray, D. Qian, D. Hsieh, Y. Xia, L. Li, J. G. Checkelsky, A. Pasupathy, K. K. Gomes, C. V. Parker, A. V. Fedorov, G. F. Chen, J. L. Luo, A. Yazdani, N. P. Ong, N. L. Wang, and M. Z. Hasan, Phys. Rev. B **78**, 184508 (2008).
[14] A. A. Kordyuk, V. B. Zabolotnyy, D. V. Evtushinsky, T. K. Kim, I. V. Morozov, M. L. Kulić, R. Follath, G. Behr, B. Büchner, and S. V. Borisenko, Phys. Rev. B **83**, 134513 (2011).
[15] K. Terashima, Y. Sekiba, J. H. Bowen, K. Nakayama, T. Kawahara, T. Sato, P. Richard, Y.-M. Xu, L. J. Li, G. H. Cao, Z.-A. Xu, H. Ding, and T. Takahashi, Proc. Natl. Acad. Sci. USA **106**, 7330 (2009).
[16] M. Yi, D. H. Lu, J. G. Analytis, J.-H. Chu, S.-K. Mo, R.-H. He, R. G. Moore, X. J. Zhou, G. F. Chen, J. L. Luo, N. L. Wang, Z. Hussain, D. J. Singh, I. R. Fisher, and Z.-X. Shen, Phys. Rev. B **80**, 024515 (2009).
[17] V. Brouet, F. Rullier-Albenque, M. Marsi, B. Mansart, M. Aichhorn, S. Biermann, J. Faure, L. Perfetti, A. Taleb-Ibrahimi, P. Le Févre, F. Bertran, A. Forget, and D. Colson, Phys. Rev. Lett. **105**, 087001 (2010).
[18] B. Zhou, M. Xu, Y. Zhang, G. Xu, C. He, L. X. Yang, F. Chen, B. P. Xie, X.-Y. Cui, M. Arita, K. Shimada, H. Namatame, M. Taniguchi, X. Dai, and D. L. Feng, Phys. Rev. B **83**, 035110 (2011).
[19] Q. Fan, X. P. Shen, M. Y. Li, D. W. Shen, W. Li, X. M. Xie, Q. Q. Ge, Z. R. Ye, S. Y. Tan, X. H. Niu, B. P. Xie, and D. L. Feng, Phys. Rev. B **91**, 125113 (2015).
[20] N. Xu, C. E. Matt, P. Richard, A. van Roekeghem, S. Biermann, X. Shi, S.-F. Wu, H. W. Liu, D. Chen, T. Qian, N. C. Plumb, M. Radović, H. Wang, Q. Mao, J. Du, M. Fang, J. Mesot, H. Ding, and M. Shi, Phys. Rev. B **92**, 081116(R) (2015).
[21] Q. S. Wang, Y. Shen, and J. Zhao (private communication).
[22] T. Valla, A. V. Fedorov, P. D. Johnson, P.-A. Glans, C. McGuinness, K. E. Smith, E. Y. Andrei, and H. Berger, Phys. Rev. Lett. **92**, 086401 (2004).